

Backscatter Modulation Design for Symbiotic Radio Networks

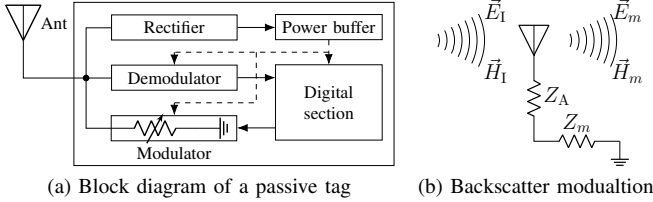


Fig. 1. For a passive tag, the rectifier and demodulator rely on the incident electromagnetic wave for energy harvesting and source decoding, while the load-switcher adjusts the reradiated signal for backscatter modulation.

I. BACKSCATTER MODEL

A. Backscatter Principles

A bistatic backscatter system consists of an excitation source, multiple (semi-)passive tags, and a backscatter reader. When illuminated, the tags simultaneously harvest energy, backscatter message, and demodulate the source signal if necessary. Fig. 1(a) shows a typical passive with a scattering antenna, an energy harvester, an integrated receiver¹, a load-switching modulator, and on-chip components (e.g., micro-controller, memory, and sensors). A portion of the impinging signal is absorbed by the tag while the remaining is backscattered to the space. According to Green's decomposition [2], the backscattered signal can be decomposed into the *structural mode* component and the *antenna mode* component. The former is fixed and depends on the antenna geometry and material properties², while the latter is adjustable and depends on the mismatch of the antenna and load impedance. Fig. 1(b) illustrates a simplified circuit and backscatter model at tag state m . The corresponding reflection coefficient is defined as³

$$\Gamma_m = \frac{Z_m - Z_A^*}{Z_m + Z_A}, \quad (1)$$

where Z_m is the load impedance at state m and Z_A is the antenna input impedance.

B. Backscatter Modulation

Backscatter modulation is achieved by switching the tag load impedance between different states. For an M -ary Quadrature Amplitude Modulation (QAM) at state $m \in \mathcal{M} \triangleq \{1, \dots, M\}$,

¹For example, [1] prototyped a compact-size pulse position demodulator based on an envelope detector, which brings great potential to coordination, synchronization, and reflection pattern control.

²The structural mode component can be regarded as part of the environment multipath and modeled by channel estimation [3].

³We assume the linear backscatter model where the reflection coefficient is irrelevant to the incident electromagnetic field at the tag [4].

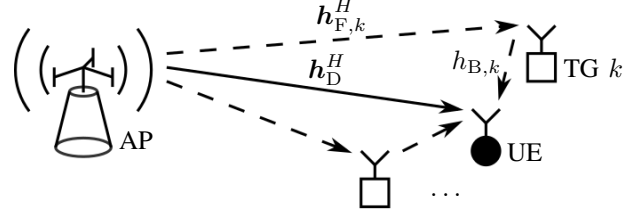


Fig. 2. A single-user multi-tag symbiotic radio system.

the reflection coefficient Γ_m maps to the signal constellation point \bar{c}_m as [5]

$$\Gamma_m = \alpha \frac{\bar{c}_m}{\max_{m'} |\bar{c}_{m'}|}, \quad (2)$$

where $\alpha \in [0, 1]$ is the reflection efficiency at a given direction. For simplicity, we consider an M -ary Phase Shift Keying (PSK) with constellation set $\mathcal{C} \triangleq \{\bar{c}_1, \dots, \bar{c}_M\}$, where the m -th constellation point is

$$\bar{c}_m = \exp\left(j \frac{2\pi m}{M}\right). \quad (3)$$

Remark 1. For passive tags, the reflection efficiency α controls the tradeoff between the harvestable power and backscatter strength: $\alpha = 0$ corresponds to maximum power transfer to the tag, while $\alpha = 1$ with M -PSK corresponds to ideal Intelligent Reflecting Surface (IRS) with M discrete states.

II. BACKSCATTER DETECTION AND ACHIEVABLE RATES

A. System Model

As shown in Fig. 2, we propose a single-user (UE) multi-tag (TG) symbiotic radio network where the Radio Frequency (RF) signal generated by the Q -antenna Access Point (AP) is shared by two coexisting systems. In the primary downlink system, the AP transmits information to the single-antenna user. In the secondary backscatter system, the AP acts as the carrier emitter, the K nearby single-antenna tags modulate their information over the reradiated RF signals, and the user serves as the multi-tag backscatter reader. Denote the AP-UE direct channel as $\mathbf{h}_D^H \in \mathbb{C}^{1 \times Q}$, the AP-TG $k \in \mathcal{K} \triangleq \{1, \dots, K\}$ forward channel as $\mathbf{h}_{F,k}^H \in \mathbb{C}^{1 \times Q}$, the TG k -UE backward channel as $h_{B,k}$, and the cascaded forward-backward channel of tag k as $\mathbf{h}_{C,k}^H \triangleq h_{B,k} \mathbf{h}_{F,k}^H \in \mathbb{C}^{1 \times Q}$. For simplicity, we consider a quasi-static block fading model where the channel coefficients remain constant within each coherence interval and vary independently over different coherence intervals, and assume the coherence interval T is much longer than the backscatter symbol period T_c and primary symbol period T_s . We also assume the direct channel and all cascaded channels can be successfully estimated

and fed back to the AP.⁴ Since the tags need to physically switch the loads for backscatter modulation, they communicate at a much longer symbol period (and lower rates) than the primary system. As such, we assume the transitions of all tags are perfectly synchronized, and the backscatter symbol period satisfies $T_c = NT_s$ where $N \gg 1$ is a positive integer.

Without loss of generality, we focus on the transmissions and detections during one particular backscatter symbol period. To provide a preliminary insight, we assume the primary symbol $s[n]$ at block $n \in \mathcal{N} \triangleq \{1, \dots, N\}$ is in standard Circularly Symmetric Complex Gaussian (CSCG) distribution, and the backscatter symbol c_k of tag k employs M -PSK modulation by (3), i.e., $c_k \in \mathcal{C}$, $\forall k \in \mathcal{K}$. Thus, the signal received by the user at block n can be expressed as⁵

$$y[n] = \left(\mathbf{h}_D^H + \sum_{k \in \mathcal{K}} \sqrt{\alpha_k} \mathbf{h}_{C,k}^H c_k \right) \mathbf{w} s[n] + w[n], \quad (4)$$

where $\mathbf{w} \in \mathbb{C}^{Q \times 1}$ is the active precoder satisfying $\|\mathbf{w}\|^2 \leq P$, P is the average transmit power constraint at the AP, and $w[n] \sim \mathcal{CN}(0, \sigma_w^2)$ is the equivalent Additive White Gaussian Noise (AWGN) at block n . Besides, we collect the backscatter symbols of K tags into $c_{\mathcal{K}} \triangleq \{c_k : k \in \mathcal{K}\}$, stack the received signal over N blocks as $\mathbf{y} \triangleq [y[1], \dots, y[N]]^T \in \mathbb{C}^{N \times 1}$, and define the equivalent channel for primary transmission as

$$\mathbf{h}_E^H(c_{\mathcal{K}}) \triangleq \mathbf{h}_D^H + \sum_{k \in \mathcal{K}} \sqrt{\alpha_k} \mathbf{h}_{C,k}^H c_k. \quad (5)$$

Remark 2. The proposed symbiotic radio system includes a multiplicative Multiple Access Channel (MAC) where the AP and the tags simultaneously transmit to the user. It inspired [TODO] to perform Successive Interference Cancellation (SIC) that first non-coherently detects the primary message under backscatter uncertainty, then cancels its contribution and decodes the tag messages. This scheme requires non-coherent coding at the AP and K re-encoding, precoding, and subtraction operations at the user. However, different from the conventional MAC with Superposition Coding (SC), the symbiotic radio system involves Multiplication Coding (MC) that combines the primary and secondary messages by multiplication. Hence, novel multi-stream detection techniques should be tailored to symbiotic radio systems to accommodate the massive connectivity of tags and the multiplicative combination of links.

B. Backscatter Detection

To reveal the impact of backscatter modulation on the primary transmission and avoid the exponential complexity of joint detection, we extend the non-coherent Ambient Backscatter Communications (AmBC) detection [11] to the multi-tag case, and propose a low-complexity energy detection to decode the backscatter symbols under primary source uncertainty. It

⁴Due to the lack of RF chains at the passive tag, accurate and efficient Channel State Information (CSI) acquisition at the AP can be challenging. One possible approach is that the AP sends pre-defined pilots, the tags respond in well-designed manners, and the user performs least-square estimation with feedbacks [6]–[8].

⁵We omit the signal reflected by two or more times [9] and assume the time difference of arrival from different paths are negligible [10].

requires no dedicated receivers or non-coherent codes at the AP, and can be readily implemented over legacy downlink systems.

Remark 3. One key property of symbiotic radio is the primary message propagates to the user from a known channel and multiple multiplicative channels with uncertainty introduced by backscatter modulation. As such, each reflection coefficient simultaneously encodes the tag message and influences the equivalent channel of the primary link. If the backscatter symbols can be successfully decoded first, they can be modeled within the equivalent channel (5) as in channel training, instead of being removed by SIC.

To explicitly specify the instances of the backscatter symbols, we define the modulation index set as $m_{\mathcal{K}} \triangleq \{m_k \in \mathcal{M} : k \in \mathcal{K}\}$ and label the corresponding tag input combination as $\bar{c}_{m_{\mathcal{K}}} \triangleq \{\bar{c}_{m_k} \in \mathcal{C} : m_k \in \mathcal{M}, k \in \mathcal{K}\}$. Since any $\bar{c}_{m_{\mathcal{K}}}$ remains constant per N primary symbols, the received signal at block n is only subject to the variation of the primary source $s[n]$ and AWGN $w[n]$, and thus follows CSCG distribution $y_{m_{\mathcal{K}}}[n] \sim \mathcal{CN}(0, \sigma_{m_{\mathcal{K}}}^2)$, where the variance

$$\sigma_{m_{\mathcal{K}}}^2 = \left| \underbrace{\left(\mathbf{h}_D^H + \sum_{k \in \mathcal{K}} \sqrt{\alpha_k} \mathbf{h}_{C,k}^H \bar{c}_{m_k} \right) \mathbf{w}}_{\mathbf{h}_E^H(\bar{c}_{m_{\mathcal{K}}})} \right|^2 + \sigma_w^2, \quad (6)$$

denotes the expectation of the received power per primary block under tag modulation index set $m_{\mathcal{K}}$. For the ease of exposition, we denote the hypothesis that the tag input combination at status $i \in \mathcal{M}^{\mathcal{K}} \triangleq \{1, \dots, M^K\}$ as \mathcal{H}_i , sort $\{\sigma_{m_{\mathcal{K}}}^2\}$ in ascending order by a one-to-one mapping $m_{\mathcal{K}} \mapsto i$,⁶ define the received signal energy over N primary blocks as $z \triangleq \|\mathbf{y}\|^2$, and let $f(z | \mathcal{H}_i)$ be the conditional probability density function of receiving z under hypothesis \mathcal{H}_i . Correspondingly, z is the sum of N i.i.d. exponential variables each with mean σ_i^2 , and the conditional probability density function follows Erlang distribution with shape N and scale σ_i^2 as

$$f(z | \mathcal{H}_i) = \frac{z^{N-1} e^{-z/\sigma_i^2}}{\sigma_i^{2N} (N-1)!}. \quad (7)$$

Remark 4. The backscatter links essentially form a discrete-input continuous-output memoryless channel. To further reduce decoding complexity, we apply hard-decision detection and construct a Discrete Memoryless Thresholding Channel (DMTC), whose capacity is a function of both input distribution and decision thresholds [12].

Denote the decision region of hypothesis \mathcal{H}_i as

$$\mathcal{R}_i \triangleq [T_{i-1,i}, T_{i,i+1}), \quad (8)$$

where $T_{i-1,i}$ is the decision threshold between \mathcal{H}_{i-1} and \mathcal{H}_i , and $T_{i,i+1}$ is the decision threshold between \mathcal{H}_i and \mathcal{H}_{i+1} . We also define $T_{0,1} \triangleq 0$, $T_{M^K, M^K+1} \triangleq \infty$, and $\mathbf{t} \triangleq [T_{0,1}, \dots, T_{M^K, M^K+1}]^T \in \mathbb{R}^{(M^K+1) \times 1}$.

⁶When more than one modulation index sets yield the same energy level, the mapping is not unique and the detection fails to separate them. This blind spot issue can be mitigated by multi-antenna techniques.

Consider the (Maximum-Likelihood (ML)) detector for example. The likelihood ratio between hypotheses \mathcal{H}_i and $\mathcal{H}_{i'}$ is [11]

$$\Lambda_{i,i'}^{\text{ML}}(z) = \frac{f(z | \mathcal{H}_i)}{f(z | \mathcal{H}_{i'})} = \left(\frac{\sigma_{i'}^2}{\sigma_i^2} \right)^N \exp \left(\frac{\sigma_i^2 - \sigma_{i'}^2}{\sigma_i^2 \sigma_{i'}^2} z \right), \quad (9)$$

the corresponding decision rule is

$$\Lambda_{i,i'}^{\text{ML}}(z) \stackrel{\mathcal{H}_i}{\leq} 1 \iff z \stackrel{\mathcal{H}_i}{\leq} T_{i,i'}^{\text{ML}}, \quad (10)$$

and the detection threshold is

$$T_{i,i'}^{\text{ML}} \triangleq N \frac{\sigma_i^2 \sigma_{i'}^2}{\sigma_i^2 - \sigma_{i'}^2} \log \frac{\sigma_i^2}{\sigma_{i'}^2}. \quad (11)$$

Remark 5. Although the ML decision threshold is optimal in terms of the likelihood function, it is not necessarily capacity-achieving, although the performance gap can be negligible in the single-tag Binary-Input Binary-Output (BIBO) case.

Once the decision region is determined, we can formulate an equivalent point-to-point Discrete Memoryless Channel (DMC) from tag input combination alphabet \mathcal{M}^K to output energy level alphabet \mathcal{M}^K . The probability of receiving energy level j under tag input combination i is⁷

$$P(\bar{z}_j | \bar{c}_i) = P(z \in \mathcal{R}_j | \mathcal{H}_i) = \int_{\mathcal{R}_j} f(z | \mathcal{H}_i) dz. \quad (12)$$

On top of this, we can compute the marginal probability of each tag and obtain K transition matrices from \mathcal{M} to \mathcal{M}^K that compose a discrete memoryless MAC. The probability of observing energy level j when tag k at status m_k is

$$P(\bar{z}_j | \bar{c}_{m_k}) = \frac{\sum_{m_K \setminus \{k\}} P(\bar{z}_j | \bar{c}_{m_K})}{\sum_{m_K} P(\bar{z}_j | \bar{c}_{m_K})}. \quad (13)$$

In summary, with the CSI knowledge and for any given precoder and detection threshold set, we can obtain the expected power of the received signal per block by (6), the conditional probability density function of the accumulated energy by (7), the decision region by (8), the equivalent point-to-point channel by (12), and the discrete memoryless MAC by (13).

C. Sum backscatter rate

We first introduce some prerequisites of information theory. Define the input probability distribution of tag k at status m_k as $P_k(\bar{c}_{m_k})$, and let $\mathbf{p}_k \triangleq [P_k(\bar{c}_1), \dots, P_k(\bar{c}_M)]^T \in \mathbb{R}^{M \times 1}$, $\mathbf{P} \triangleq [\mathbf{p}_1^T, \dots, \mathbf{p}_K^T]^T \in \mathbb{R}^{M \times K}$. Assume the input distribution of all tags are mutually independent such that $P_K(\bar{c}_{m_K}) = \prod_{k \in \mathcal{K}} P_k(\bar{c}_{m_k})$. Following [13], the backscatter information function associated with tag input combination \bar{c}_{m_K} is defined as

$$I_B(\bar{c}_{m_K}; z) \triangleq \sum_j P(\bar{z}_j | \bar{c}_{m_K}) \log \frac{P(\bar{z}_j | \bar{c}_{m_K})}{P(\bar{z}_j)}, \quad (14)$$

⁷For simplicity, we assume there exists at least one feasible precoder that produces distinct received energy levels for all tag input combinations. [TODO] Merge with precoder design.

the backscatter marginal information function of tag $q \in \mathcal{K}$ associated with \bar{c}_{i_q} , $i_q \in \mathcal{M}$ is defined as

$$I_{B,q}(\bar{c}_{i_q}; z) \triangleq \sum_{m_K \setminus \{q\}} \prod_{k \in \mathcal{K} \setminus \{q\}} P_k(\bar{c}_{m_k}) I_B(\bar{c}_{m_K \setminus \{q\}}, \bar{c}_{i_q}; z), \quad (15)$$

and the backscatter mutual information can be expressed as⁸

$$\begin{aligned} I_B(c_K; z) &= \mathbb{E}_{c_K} [I_B(\bar{c}_{m_K}; z)] = \mathbb{E}_{c_K} [I_{B,k}(\bar{c}_{m_k}; z)] \quad (16a) \\ &= \sum_{m_K} \prod_{k \in \mathcal{K}} P_k(\bar{c}_{m_k}) \sum_j P(\bar{z}_j | \bar{c}_{m_K}) \log \frac{P(\bar{z}_j | \bar{c}_{m_K})}{P(\bar{z}_j)}. \quad (16b) \end{aligned}$$

Evidently, (14)–(16) are functions of the tag input distribution \mathbf{P} as well as the discrete memoryless MAC $P(z | c_K)$, and thus depend on the transmit precoder \mathbf{w} and the detection threshold t .

D. Ergodic primary rate

Once the tag input combination is successfully decoded, the user can eliminate backscatter uncertainty and model its contribution within the equivalent primary channel (5). As such, the tags can adjust the propagation environment in a potentially beneficial manner, and create artificial channel variation within each fading block. Similarly, we define the primary information function associated with tag input combination \bar{c}_{m_K} and the primary marginal information function of tag q associated with symbol \bar{c}_{i_q} respectively as

$$I_P(\bar{c}_{m_K}; \mathbf{y}) \triangleq N \log_2 \left(1 + \frac{|\mathbf{h}_E^H(\bar{c}_{m_K}) \mathbf{w}|^2}{\sigma_w^2} \right), \quad (17)$$

$$I_{P,q}(\bar{c}_{i_q}; \mathbf{y}) \triangleq \sum_{m_K \setminus \{q\}} \prod_{k \in \mathcal{K} \setminus \{q\}} P_k(\bar{c}_{m_k}) I_P(\bar{c}_{m_K \setminus \{q\}}, \bar{c}_{i_q}; \mathbf{y}), \quad (18)$$

and the ergodic primary rate can be expressed as⁹

$$I_P(c_K; \mathbf{y}) = \mathbb{E}_{c_K} [I_P(\bar{c}_{m_K}; \mathbf{y})] = \mathbb{E}_{c_K} [I_{P,k}(\bar{c}_{m_k}; \mathbf{y})] \quad (19a)$$

$$= \sum_{m_K} \prod_{k \in \mathcal{K}} P_k(\bar{c}_{m_k}) N \log_2 \left(1 + \frac{|\mathbf{h}_E^H(\bar{c}_{m_K}) \mathbf{w}|^2}{\sigma_w^2} \right). \quad (19b)$$

In contrast to the backscatter case, (17)–(19) are irrelevant to the detection threshold t , but depend on the tag input probability distribution \mathbf{P} and the transmit precoder \mathbf{w} .

III. INPUT DISTRIBUTION, DECISION REGION, AND PRECODER DESIGN

A. Primary-backscatter rate region

The weighted sum marginal information of tag q associated with symbol \bar{c}_{i_q} and the weighted sum primary-backscatter rate are defined respectively as

$$I_q(\bar{c}_{i_q}; \mathbf{y}, z) \triangleq \rho I_{P,q}(\bar{c}_{i_q}; \mathbf{y}) + (1 - \rho) I_{B,q}(\bar{c}_{i_q}; z), \quad (20)$$

$$I(c_K; \mathbf{y}, z) \triangleq \rho I_P(c_K; \mathbf{y}) + (1 - \rho) I_B(c_K; z), \quad (21)$$

⁸Please be aware that c_K , c_k , z are random variables, while \bar{c}_{m_K} and \bar{c}_i , \bar{c}_{m_k} , \bar{z}_j represent the corresponding instances.

⁹The unit of (14)–(16) are bit per channel use (bpcu), while the unit of (17)–(19) are bit per second per Hertz (bps/Hz).

where $\rho \in [0, 1]$ denotes the priority of the primary link. To investigate how backscatter modulation and detection may influence the primary transmission, we optimize the input probability distribution, decision region, and transmit precoder to maximize the weighted primary-backscatter sum rate

$$\max_{\mathbf{P}, \mathbf{t}, \mathbf{w}} I \quad (22a)$$

$$\text{s.t.} \quad \sum_{m_k} P_k(\bar{c}_{m_k}) = 1, \quad \forall k \in \mathcal{K}, \quad (22b)$$

$$P_k(\bar{c}_{m_k}) \geq 0, \quad \forall m_k \in \mathcal{M}, \quad \forall k \in \mathcal{K}, \quad (22c)$$

$$\|\mathbf{w}\|^2 \leq P. \quad (22d)$$

where (22b) and (22c) are input probability constraints and (22d) is the average transmit power budget. As problem (22) is not jointly convex over \mathbf{P} , \mathbf{t} and \mathbf{w} , we propose a Block Coordinate Descent (BCD) method that iteratively updates the input distribution, decision region, and transmit precoder, until convergence is achieved.

B. Input probability distribution

For any fixed decision boundary \mathbf{t} and transmit precoder \mathbf{w} , the equivalent discrete memoryless MAC can be determined by (13) and problem (22) boils down to

$$\max_{\mathbf{P}} I \quad (23a)$$

$$\text{s.t.} \quad (22b), (22c), \quad (23b)$$

which is non-convex for $K > 1$ due to the product term $\prod_{k \in \mathcal{K}} P_k(\bar{c}_{m_k})$. Fortunately, the Karush–Kuhn–Tucker (KKT) conditions are sufficient and necessary for this type of problem, and the proof follows straightforwardly from [14].¹⁰ Denote the Lagrange multiplier associated with (22b) and (22c) as $\boldsymbol{\mu} \triangleq [\mu_1, \dots, \mu_K]^T \in \mathbb{R}^{K \times 1}$ and $\boldsymbol{\Lambda} \triangleq [\boldsymbol{\lambda}_1^T, \dots, \boldsymbol{\lambda}_K^T]^T \in \mathbb{R}^{M \times K}$ with $\boldsymbol{\lambda}_k \triangleq [\lambda_{k,1}, \dots, \lambda_{k,M}]^T \in \mathbb{R}^{M \times 1}$, respectively. The Lagrangian function of problem (23) is

$$J = -I + \sum_{k \in \mathcal{K}} \mu_k \left(\sum_{m_k \in \mathcal{M}} P_k(\bar{c}_{m_k}) - 1 \right) - \sum_{k \in \mathcal{K}} \sum_{m_k \in \mathcal{M}} \lambda_{k,m_k} P_k(\bar{c}_{m_k}), \quad (24)$$

and the corresponding KKT conditions on the primal and dual solutions are, $\forall i_q \in \mathcal{M}$ and $\forall q \in \mathcal{K}$,

$$-\frac{\partial I}{\partial P_q^*(\bar{c}_{i_q})} + \mu_q^* - \lambda_{q,i_q}^* = 0, \quad (25a)$$

$$\lambda_{q,i_q}^* = 0, \quad P_q^*(\bar{c}_{i_q}) > 0, \quad (25b)$$

$$\lambda_{q,i_q}^* \geq 0, \quad P_q^*(\bar{c}_{i_q}) = 0. \quad (25c)$$

¹⁰For any elementary discrete memoryless MAC (sizes of input alphabets are no greater than that of output alphabet), the sufficiency can be proved by combining the local maximum and connectedness of KKT solutions. For any general discrete memoryless MAC, the capacity can be achieved by an elementary discrete memoryless MAC included within. Thus, we restrict the discussion of this paper to elementary discrete memoryless MACs.

The partial derivative can be explicitly expressed as

$$\frac{\partial I}{\partial P_q^*(\bar{c}_{i_q})} = \rho I_{P,q}(\bar{c}_{i_q}; \mathbf{y}) + (1 - \rho) (I_{B,q}(\bar{c}_{i_q}; z) - 1) \quad (26a)$$

$$= I_q(\bar{c}_{i_q}; \mathbf{y}, z) - (1 - \rho), \quad (26b)$$

which suggests μ_q^* must satisfy

$$\mu_q^* = I_q(\bar{c}_{i_q}; \mathbf{y}, z) - (1 - \rho), \quad P_q^*(\bar{c}_{i_q}) > 0, \quad (27a)$$

$$\mu_q^* \geq I_q(\bar{c}_{i_q}; \mathbf{y}, z) - (1 - \rho), \quad P_q^*(\bar{c}_{i_q}) = 0. \quad (27b)$$

Due to the sufficiency and necessity of the KKT conditions, we can conclude that any input probability distribution \mathbf{P}^* maximizes the weighted sum primary-backscatter rate if and only if, $\forall i_q \in \mathcal{M}$ and $\forall q \in \mathcal{K}$,

$$I_q(\bar{c}_{i_q}; \mathbf{y}, z) = C_q, \quad P_q^*(\bar{c}_{i_q}) > 0, \quad (28a)$$

$$I_q(\bar{c}_{i_q}; \mathbf{y}, z) \leq C_q, \quad P_q^*(\bar{c}_{i_q}) = 0, \quad (28b)$$

where $C_q \triangleq \mu_q^* + (1 - \rho)$. Apparently, it holds that

$$\sum_{i_q} P_q^*(\bar{c}_{i_q}) I_q(\bar{c}_{i_q}; \mathbf{y}, z) = C_q. \quad (29)$$

On the other hand, by the definition of marginations (16a), (19a) and weighted summations (20), (21), we have

$$\sum_{i_q} P_q^*(\bar{c}_{i_q}) I_q(\bar{c}_{i_q}; \mathbf{y}, z) = I(c_{\mathcal{K}}; \mathbf{y}, z), \quad (30)$$

which is irrelevant to q . Hence, $C_q = I(c_{\mathcal{K}}; \mathbf{y}, z)$, $\forall q \in \mathcal{K}$ and

$$I_q(\bar{c}_{i_q}; \mathbf{y}, z) = I(c_{\mathcal{K}}; \mathbf{y}, z), \quad P_q^*(\bar{c}_{i_q}) > 0, \quad (31a)$$

$$I_q(\bar{c}_{i_q}; \mathbf{y}, z) \leq I(c_{\mathcal{K}}; \mathbf{y}, z), \quad P_q^*(\bar{c}_{i_q}) = 0. \quad (31b)$$

It suggests that an input probability distribution maximizes the weighted primary-backscatter sum rate if and only if each probable state of each tag produces the same mutual information.

C. Decision region

As indicated by [15], the optimal ML decision regions are very close to the optimal decision regions to problem (22). We can either use (8) as suboptimal, or take derivative of (16) w.r.t. $T_{i-1,i}$ and $T_{i,i+1}$ (however, closed-form solutions are unavailable and two-dimensional search is needed).

D. Precoder

Interestingly, we can design precoder to adjust the expectation of the received power (6) at each tag input combination, which can avoid the detection blind spots in [11] and further boost the weighted sum-rate. However, the problem is highly

non-convex – the information function associated with input combination status i is

$$I(\bar{c}_i; z) = \sum_{j \in \mathcal{M}^K} \int_{T_{j-1,j}}^{T_{j,j+1}} \frac{z^{N-1} \exp\left(-\frac{z}{\text{tr}(H_{E,i}W) + \sigma_w^2}\right)}{(\text{tr}(H_{E,i}W) + \sigma_w^2)^N (N-1)!} dz \\ \times \log \frac{\int_{T_{j-1,j}}^{T_{j,j+1}} \frac{z^{N-1} \exp\left(-\frac{z}{\text{tr}(H_{E,i}W) + \sigma_w^2}\right)}{(\text{tr}(H_{E,i}W) + \sigma_w^2)^N (N-1)!} dz}{\sum_{i' \in \mathcal{M}^K} \int_{T_{j-1,j}}^{T_{j,j+1}} \frac{z^{N-1} \exp\left(-\frac{z}{\text{tr}(H_{E,i'}W) + \sigma_w^2}\right)}{(\text{tr}(H_{E,i'}W) + \sigma_w^2)^N (N-1)!} dz}, \quad (32)$$

and the mutual information can be expressed as a function of W by combining (16) and (32).

So far I have no idea how to solve this issue, and found no reference regarding precoder design for AmBC/Symbiotic Radio (SR) with discrete channels (although some naive combiner designs are available for BIBO). Personally, I believe the precoder design is the key to (i) boost the rate region and avoid blind spots in conventional AmBC; (ii) build our proposal over existing infrastructures. Ideally, assuming the number of transmit antennas Q is larger than the number of tags K , the optimal energy levels should be almost uniformly spaced (as z follows Erlang distribution) to concentrate the channel transitional probability on diagonal as possible.

REFERENCES

- [1] J. Kim and B. Clerckx, “Wireless Information and Power Transfer for IoT: Pulse Position Modulation, Integrated Receiver, and Experimental Validation,” *arXiv:2104.08404*, pp. 1–15, apr 2021. [Online]. Available: <http://arxiv.org/abs/2104.08404>
- [2] R. Hansen, “Relationships Between Antennas as Scatterers and as Radiators,” *Proceedings of the IEEE*, vol. 77, no. 5, pp. 659–662, may 1989. [Online]. Available: <http://ieeexplore.ieee.org/document/32056/>
- [3] C. Boyer and S. Roy, “Backscatter Communication and RFID: Coding, Energy, and MIMO Analysis,” *IEEE Transactions on Communications*, vol. 62, no. 3, pp. 770–785, mar 2014. [Online]. Available: <http://ieeexplore.ieee.org/document/6685977/>
- [4] Daniel Dobkin, *The RF in RFID: Passive UHF RFID in Practice*. London, U.K.: Newnes, nov 2012. [Online]. Available: <https://www.elsevier.com/books/the-rf-in-rfid/dobkin/978-0-12-394583-9>
- [5] S. J. Thomas, E. Wheeler, J. Teizer, and M. S. Reynolds, “Quadrature Amplitude Modulated Backscatter in Passive and Semipassive UHF RFID Systems,” *IEEE Transactions on Microwave Theory and Techniques*, vol. 60, no. 4, pp. 1175–1182, apr 2012. [Online]. Available: <http://ieeexplore.ieee.org/document/6153042/>
- [6] D. Bharadia, K. R. Joshi, M. Kotaru, and S. Katti, “BackFi: High Throughput WiFi Backscatter,” in *Proceedings of the 2015 ACM Conference on Special Interest Group on Data Communication*, vol. 45, no. 4. New York, NY, USA: ACM, aug 2015, pp. 283–296. [Online]. Available: <https://dl.acm.org/doi/10.1145/2785956.2787490>
- [7] G. Yang, C. K. Ho, and Y. L. Guan, “Multi-Antenna Wireless Energy Transfer for Backscatter Communication Systems,” *IEEE Journal on Selected Areas in Communications*, vol. 33, no. 12, pp. 2974–2987, dec 2015. [Online]. Available: <http://ieeexplore.ieee.org/document/7274644/>
- [8] H. Guo, Q. Zhang, S. Xiao, and Y.-C. Liang, “Exploiting Multiple Antennas for Cognitive Ambient Backscatter Communication,” *IEEE Internet of Things Journal*, vol. 6, no. 1, pp. 765–775, feb 2019. [Online]. Available: <https://ieeexplore.ieee.org/document/8411483/>
- [9] Q. Wu and R. Zhang, “Intelligent Reflecting Surface Enhanced Wireless Network via Joint Active and Passive Beamforming,” *IEEE Transactions on Wireless Communications*, vol. 18, no. 11, pp. 5394–5409, nov 2019. [Online]. Available: <https://ieeexplore.ieee.org/document/8811733/>
- [10] H. Guo, Y.-C. Liang, R. Long, and Q. Zhang, “Cooperative Ambient Backscatter System: A Symbiotic Radio Paradigm for Passive IoT,” *IEEE Wireless Communications Letters*, vol. 8, no. 4, pp. 1191–1194, aug 2019. [Online]. Available: <https://ieeexplore.ieee.org/document/8692391/>
- [11] J. Qian, A. N. Parks, J. R. Smith, F. Gao, and S. Jin, “IoT Communications With M-PSK Modulated Ambient Backscatter: Algorithm, Analysis, and Implementation,” *IEEE Internet of Things Journal*, vol. 6, no. 1, pp. 844–855, feb 2019. [Online]. Available: <https://ieeexplore.ieee.org/document/8423609/>
- [12] T. Nguyen, Y.-J. Chu, and T. Nguyen, “On the Capacities of Discrete Memoryless Thresholding Channels,” in *2018 IEEE 87th Vehicular Technology Conference (VTC Spring)*, vol. 2018-June. IEEE, jun 2018, pp. 1–5. [Online]. Available: <https://ieeexplore.ieee.org/document/8417506/>
- [13] M. Rezaeian and A. Grant, “Computation of Total Capacity for Discrete Memoryless Multiple-Access Channels,” *IEEE Transactions on Information Theory*, vol. 50, no. 11, pp. 2779–2784, nov 2004. [Online]. Available: <http://ieeexplore.ieee.org/document/1347364/>
- [14] Y. Watanabe and K. Kamoi, “A Formulation of the Channel Capacity of Multiple-Access Channel,” *IEEE Transactions on Information Theory*, vol. 55, no. 5, pp. 2083–2096, may 2009. [Online]. Available: <http://ieeexplore.ieee.org/document/4839058/>
- [15] J. Qian, Y. Zhu, C. He, F. Gao, and S. Jin, “Achievable Rate and Capacity Analysis for Ambient Backscatter Communications,” *IEEE Transactions on Communications*, vol. 67, no. 9, pp. 6299–6310, sep 2019. [Online]. Available: <https://ieeexplore.ieee.org/document/8721108/>